Dr. Marios Maroudas

Working Group: J. M. Batllori, Y. Gu, D. Horns, M. Maroudas, J. Ulrichs

WISPFI: WISP Searches on a Fiber Interferometer

Motivation

- **Axions** solve the strong CP problem and are prominent candidates for CDM [1].
- Haloscopes sensitive in μeV but depend on the ρ_{DM} → poorly constrained → could be substantially smaller [2].
- LSTW experiments not sensitive to QCD axions (conversion ∝ $g^4_{a\gamma\gamma}$).
- **High m_a range** (meV to eV) unexplored by direct detection experiments (except CAST [3]) + very difficult for resonators like cavities.
- Null results of direct DM searches → Need for **novel approaches**!

https://cajohare.github.io/AxionLimits/docs/ap.html

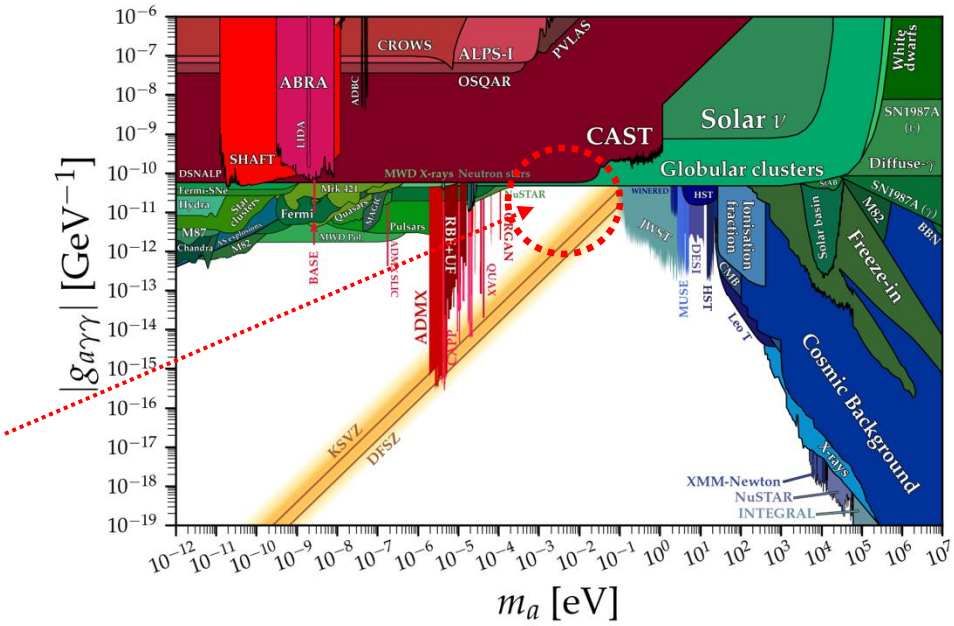

WISPFI (WISP searches on a Fiber Interferometer)

- γ→a conversion inside a **waveguide** measuring **photon disappearance** in the presence of B_{ext} [4].
- Axion conversion probability scales with [5]:

  For $P_{\gamma\to a} \ll 1$: $P_{\gamma\to a} \propto g_{a\gamma\gamma}^2 (BL)^2$
- **Mach-Zehnder interferometer** (MZI) with the sensing arm inside the magnetic field.
- Light guiding & **resonant detection.**
- Signal: **amplitude reduction** & **phase shift.**

- ➢ No ρ_{DM} dependence.
- ➢ Room temperature operation

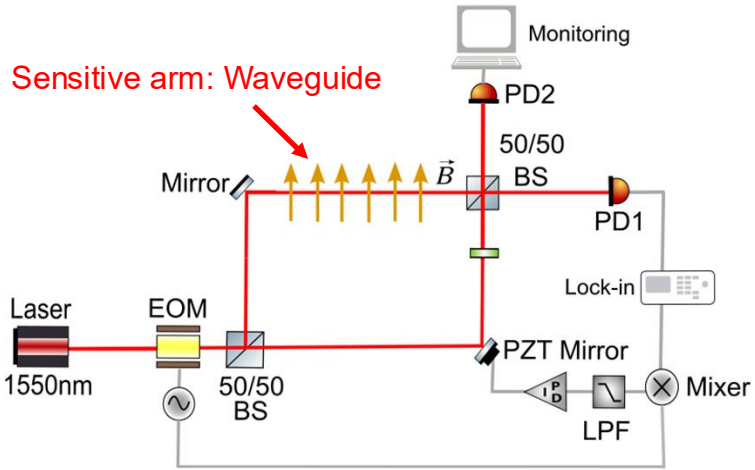

Interferometric Principle – Amplitude Modulation

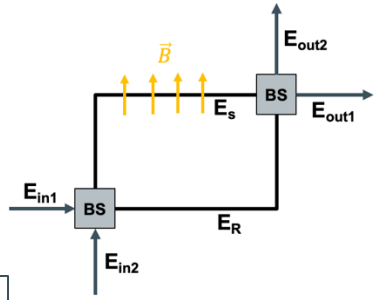

1. Input Field (Port 1 & Port 2):

$$E_{\text{in1}}(t) = \frac{E_0}{\sqrt{2}} e^{i\omega_\gamma t} e^{i\beta_m \sin(\omega_m t)}, \qquad E_{in2}(t) = 0$$

2. Split in Carrier + Sidebands:

$$E_{\text{in1}}(t) = E_{\text{car}}(t) + E_{\text{sid}}(t)$$

$$E_{\text{car}}(t) = E_0 e^{i\omega_\gamma t} \qquad E_{sid}(t) = \frac{E_0 \beta_m}{2i}\left[e^{it(\omega_\gamma + \omega_m)} - e^{it(\omega_\gamma - \omega_m)}\right]$$

3. Split 50:50 @ Beam Splitter:

$$U_{\text{BS}} = \frac{1}{\sqrt{2}} \begin{pmatrix} 1 & i \\ i & 1 \end{pmatrix}, \begin{pmatrix} E_{\text{S}} \\ E_{\text{R}} \end{pmatrix} = U_{\text{BS}} \begin{pmatrix} E_{\text{in1}} \\ E_{\text{in2}} \end{pmatrix}$$

4. Dark Fringe Conditions:

$$k_\gamma \Delta L = (2n+1)\pi + \alpha_\gamma, \quad n \in \mathbb{Z}, k_\gamma = \frac{2\pi}{\lambda_\gamma} \quad \& \quad k_m \Delta L = (2p+1)\pi + \alpha_m, \quad p \in \mathbb{Z}, k_m = \frac{\omega_m}{c}$$

For Carrier

For Sidebands

Demodulation Procedure

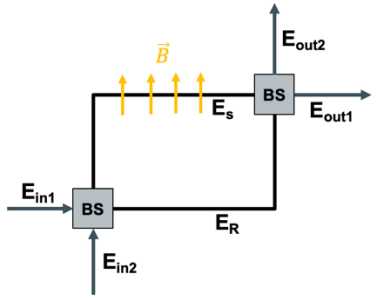

5. Output power after recombination at dark port (2) for perfect dark fringe conditions:

$$P_{out2}^{AM} = \frac{E_0^2}{4}\left[P_{\gamma\to a}^2 + \beta_m^2\left(2 - P_{\gamma\to a}\right)^2\cos^2\left(\omega_m t - k_m L\right) - 2\beta_m\left(2 - P_{\gamma\to a}\right)P_{\gamma\to a}\cos\left(\omega_m t - k_m L\right)\right]$$

carrier-carrier | sideband-sideband | carrier-sideband

$$P_{cross,out2}(t) = E_0^2\beta_m P_{\gamma\to a}\cos(\omega_m t - k_m L)$$

6. Mixing with ω_m from LO using lock-in approach:

$$P_{mix}(t) = P_{cross,out2}(t)\cos(\omega_m t + \phi_{LO})$$

Long-time integration

$$P_{av} = \frac{1}{2}E_0^2\beta_m P_{\gamma\to a}$$

➢ After mixing and time-averaging only the interference between carrier-sideband remains!

Signal Detection Procedure

- Dark port signal demodulated at ω_m and applying a LPF.
- Average over long time periods.
- Comparison spectra between magnet ON and magnet OFF.

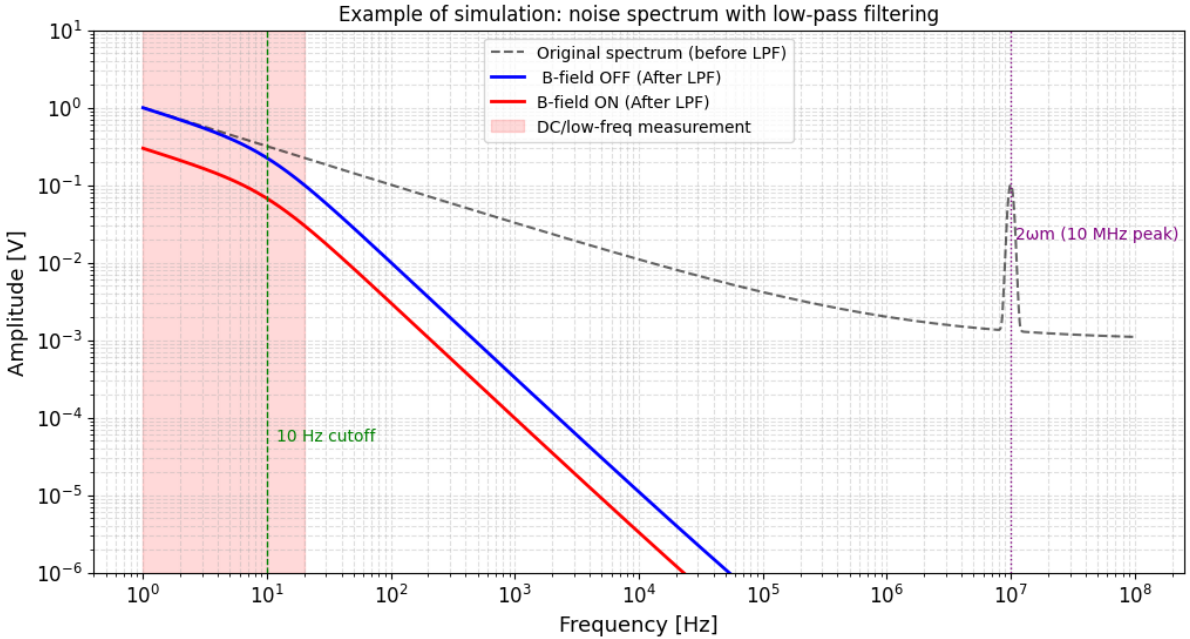

Photon-axion Conversion

$$P_{\gamma\to a} = \underbrace{\sin^2(2\theta)}_{\text{Amplitude}}\underbrace{\sin^2(\pi\, L/L_{osc})}_{\text{Oscillations}}$$ [6]

Mixing angle: $\tan(2\theta) = 2\omega\frac{g_{a\gamma\gamma}B}{k_\gamma^2 - k_a^2}$ ← Photon, axion wave momenta

- Maximum conversion occurs for **large energy ω** or at $\mathbf{k_\gamma = k_a}$ (resonant conversion, θ = 45°).
- Axion mass at resonance in a medium with effective refractive index n_{eff}:

$$m_a = \omega\sqrt{1 - n_{eff}^2}$$ → Required n_{eff} <1!

- For $P_{\gamma\to a} \ll 1$ the resulting probability becomes [5]: $P_{\gamma\to a} \approx 8x10^{-19}\left(\frac{g_{a\gamma\gamma}}{10^{-12}\ GeV^{-1}}\right)^2\left(\frac{B}{9\ T}\right)^2\left(\frac{L}{100\ m}\right)^2$

Energy (ω) independent!

Hollow-Core Photonic Crystal Fibers (HC-PCF)

- Resonant conditions can not be fulfilled for waveguides based on dielectric materials.
- HC-PCF guide light through a low-refractive index hollow core which is surrounded by a periodic arrangement of air-holes in the cladding this generating a photonic-bandgap structure [7].
- Through the bandgap structure, the propagating mode can acquire $\mathbf{n_{eff}<1}$ leading to real m_a and resonant mixing.

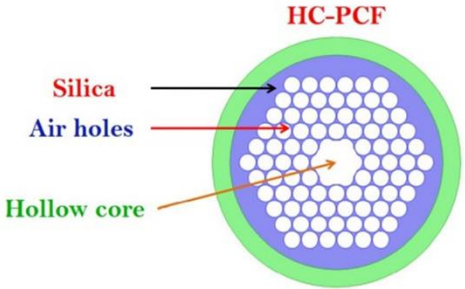

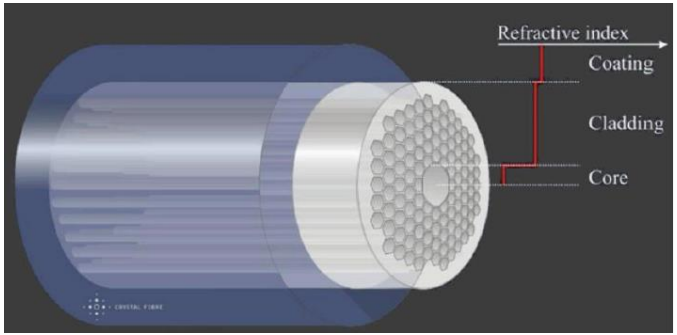

NKT Photonics

Effective mode index (n_{eff}) in HC-PCF

- n_{eff} depends on the core radius (**R_c**), the bending radius (**R_b**), and the refractive index of the effective gas (n_{gas}) which in turn depends on pressure (**p**), wavelength (**λ**), and temperature (**T**) [8, 9].

- Analytical approximations [8]: $$n_{eff} = \frac{k_\gamma}{k_o} = \sqrt{n^2_{gas}(\lambda, p, T) - \left(\frac{u_{nm}}{k_\gamma R_c}\right)^2}$$

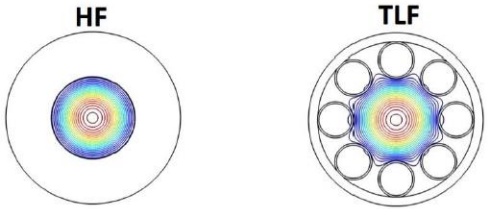

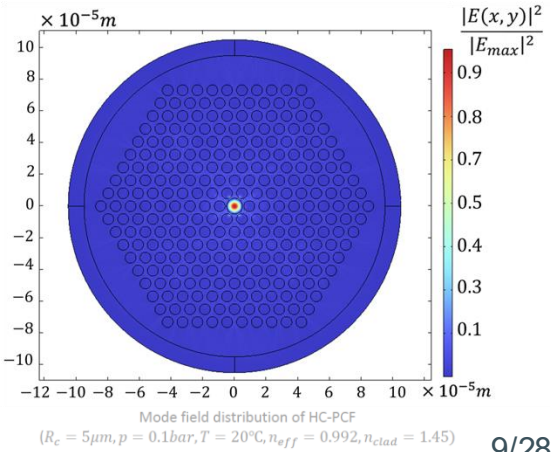

- FEM simulations studying the actual fiber geometry.

n_{eff} in HC-PCF – Core Radius Dependence

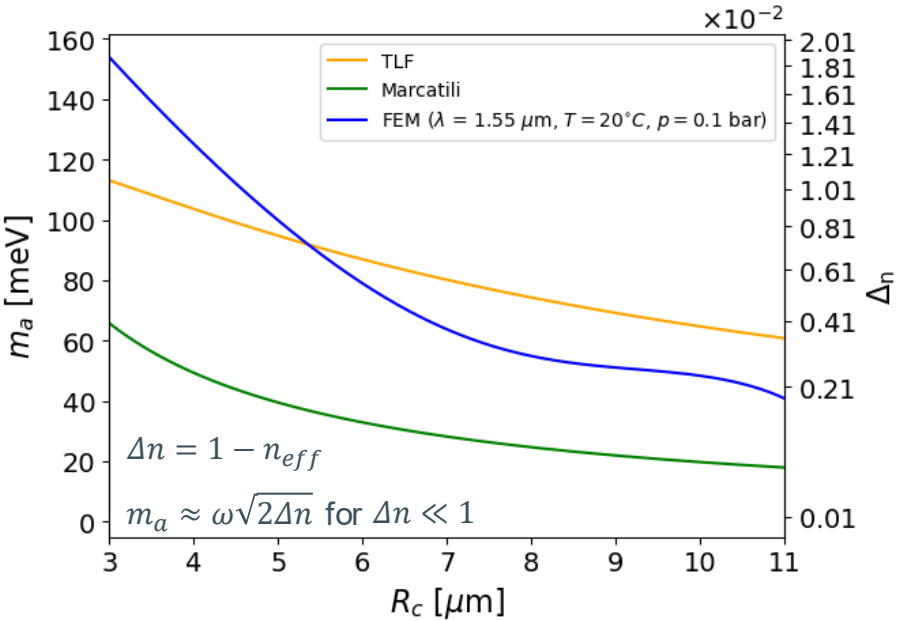

- Observed increase of n_{eff} with increasing R_c matches the analytical approximation.
- Tube-lattice fiber (TLF) model considers a hollow core surrounded by a ring of dielectric tubes. → More accurate than Marcatilli's formula which is valid only for R_c/λ >27.
- **Larger R_c → Larger n_{eff} → Smaller m_a**

n_{eff} in HC-PCF – Pressure Dependence

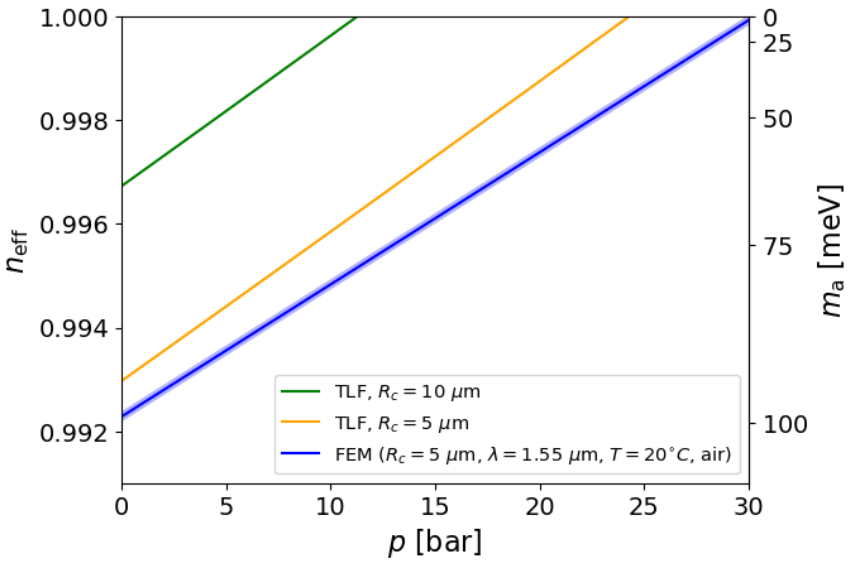

- Observed increase of n_{eff} with increasing p matches the analytical approximation.
- For R_c = 5 µm, Vacuum-like conditions for p = 30.3 bar
- For R_c = 10 µm, Vacuum-like conditions for p = 11 bar
- **Larger p → Larger n_{eff} → Smaller m_a**

n_{eff} in HC-PCF – Core Radius & Pressure Dependence

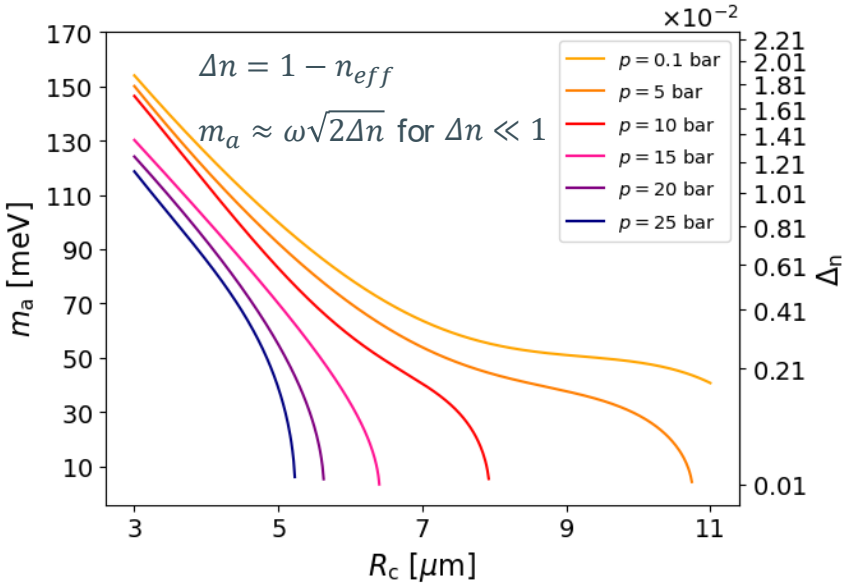

- By changing p of the air or R_c of HC-PCF we can tune the probed m_a.
- FEM simulations show that the probed m_a can range between **~ 10 meV** to **160 meV**.

n_{eff} in HC-PCF – Wavelength Dependence

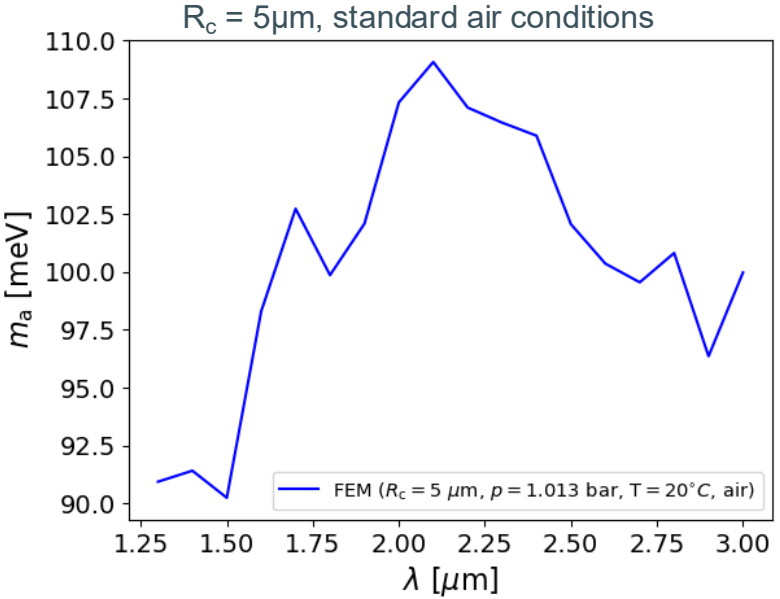

- λ of the propagating light of the fiber also have an effect on n_{eff}.
- Longer λ experience less confinement and lower n_{eff}, which can lead to lower transmission efficiency.
- **Smaller λ → Larger n_{eff} → Smaller m_a**

n_{eff} in HC-PCF – Bending Radius Dependence

R_c = 5μm, standard air conditions

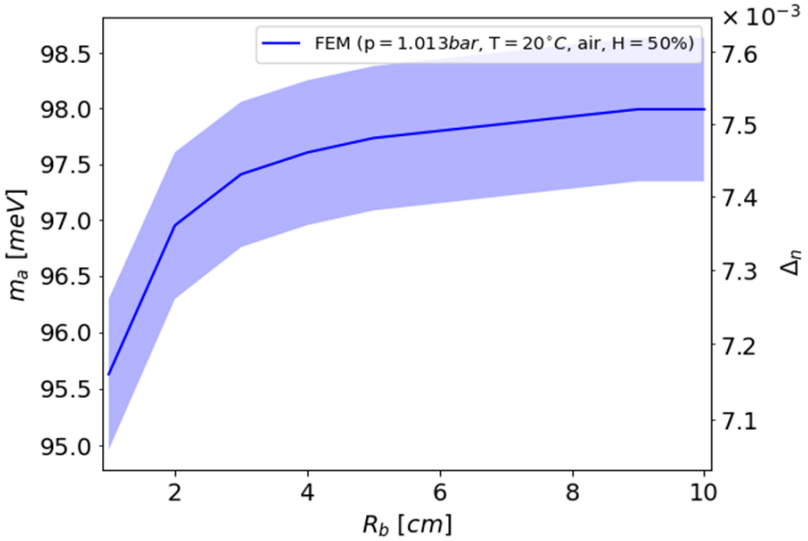

- R_b has a small effect on n_{eff} .
- Increasing bending also increases the losses.
- **Larger R_b → Smaller n_{eff} → Larger m_a**

Experimental Setup

- Partial free space, partial fiber MZI.
- Sensing arm by HC-PCF placed in the magnet bore and pressurized for tuning the probed m_a.
- Two lasers at slightly different λ + switch modulate the axion signal at ω_{sig} = 10kHz.
- EOM-AM and EOM-PM used to lock the interferometer in amplitude at ω_m = 5MHz via a PID loop.

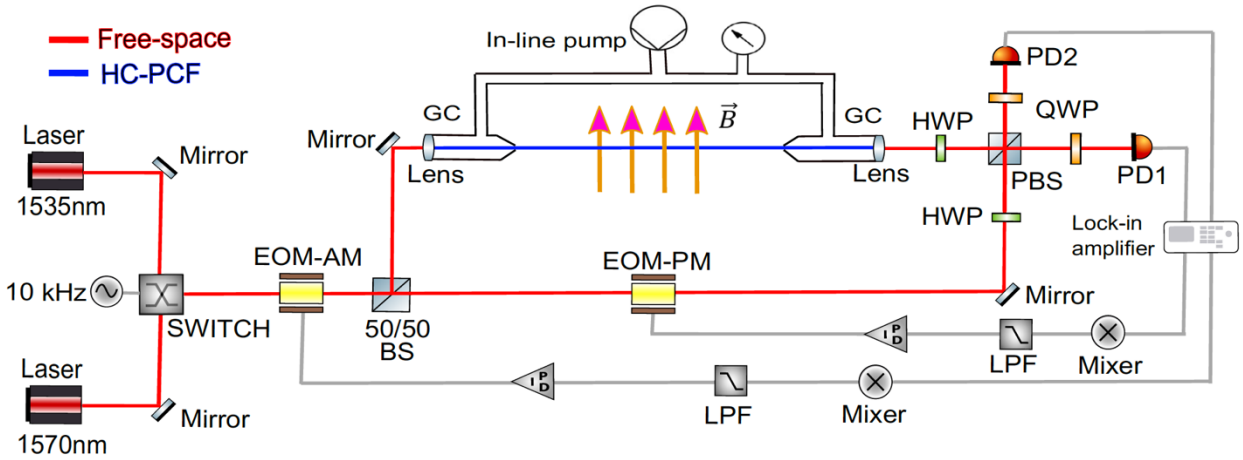

Sensitivity Estimation

- Probed m_α mainly depends on R_c.
- HC-PCF production process leads to random R_c variations (1/f).
- Variations widen the probed m_α range but reduce the sensitivity.
- Fabry Perrot cavity (FPC) with F = 100 used to increase the effective length and power on the sensing arm [10].

$$g_{a\gamma\gamma}^{(10nm)} \approx 1.79 \times 10^{-10} GeV^{-1} \left(\frac{SNR}{3}\right)^{1/2} \left(\frac{B}{9T}\right)^{-1} \left(\frac{L}{100m}\right)^{-1} *$$
$$* \left(\frac{\mathrm{F}}{100}\right)^{-1/2} \left(\frac{P_{tot}}{40W}\right)^{-1/2} \left(\frac{\beta_{sig}}{1}\right)^{-1/2} \left(\frac{\beta_m}{1}\right)^{-1/2} \left(\frac{t}{1d}\right)^{-1/4}$$
$$\left(\frac{NEP_{PD+SN}}{3fW/\sqrt{Hz}}\right)^{1/4} \left(\frac{\Delta \mathrm{v}}{10\ \mathrm{Hz}}\right)^{1/8}$$

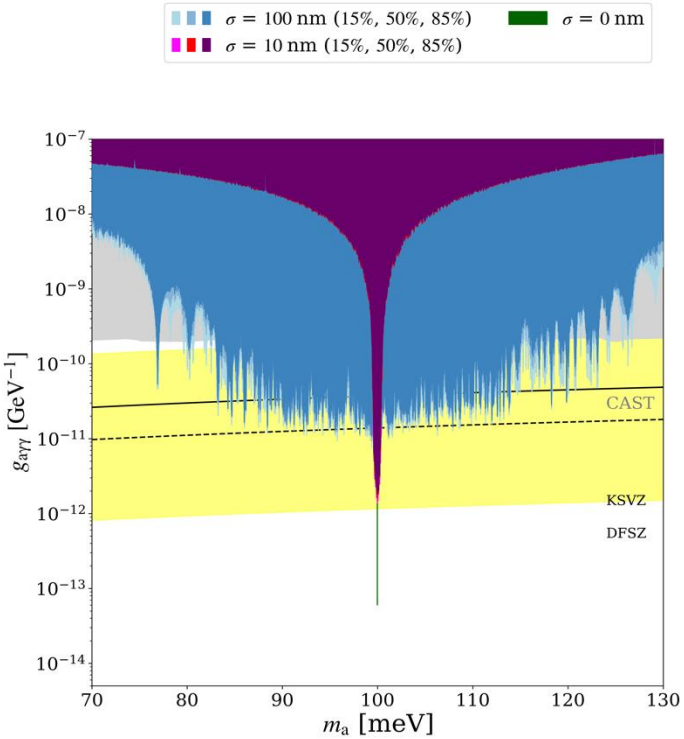

Sensitivity Estimation

- Tuning from 0.1 – 26.7 bar in 269 steps.
- Probed m_a ~ 20 – 100 meV.
- P_{tot} = 40 W laser @ λ = 1550 nm.
- B_{ext} = 9 T.
- F = 100.
- L = 100 m PM HC-PCF.
- R_c = 5 μm ± 10 nm
- t = 30 days.
- Dark Fringe = P_{dark}/P_{tot} = 1%

→ DFSZ sensitivity in a wide axion mass range!

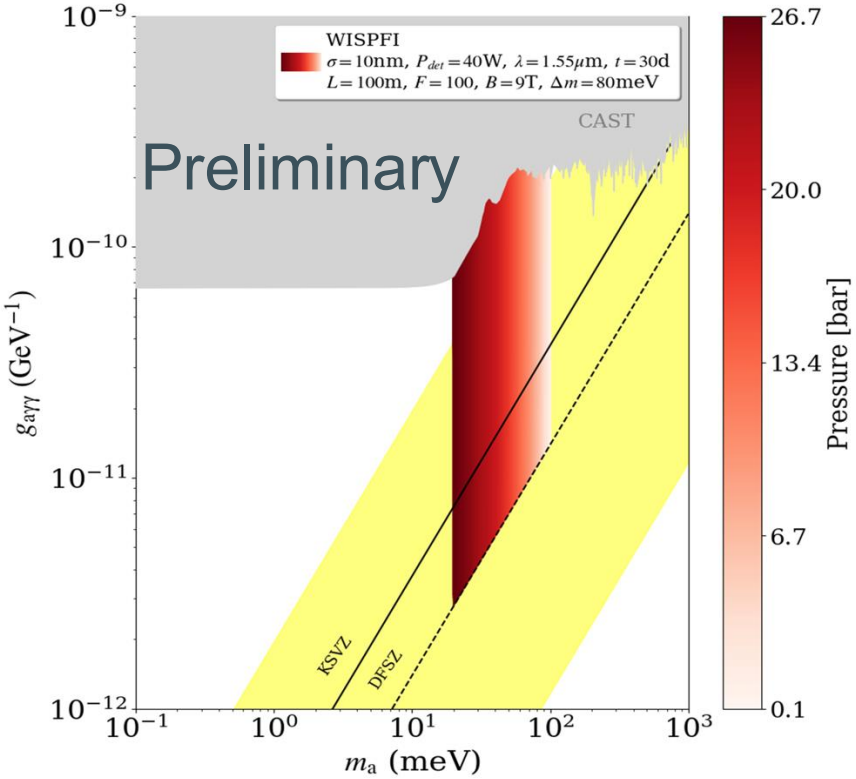

WISPFI Prototype

- Single pressure measurement at standard air conditions → No tuning.
- HC-PCF in sensing arm placed in 1 m-long permanent magnet panel.
- Phase modulation (EOM-PM1) at ω_m = 4MHz and interferometer phase-lock (EOM-PM2) via a PID loop.
- EOM-AM setting a different frequency (5MHz) for measuring axion-induced amplitude changes.

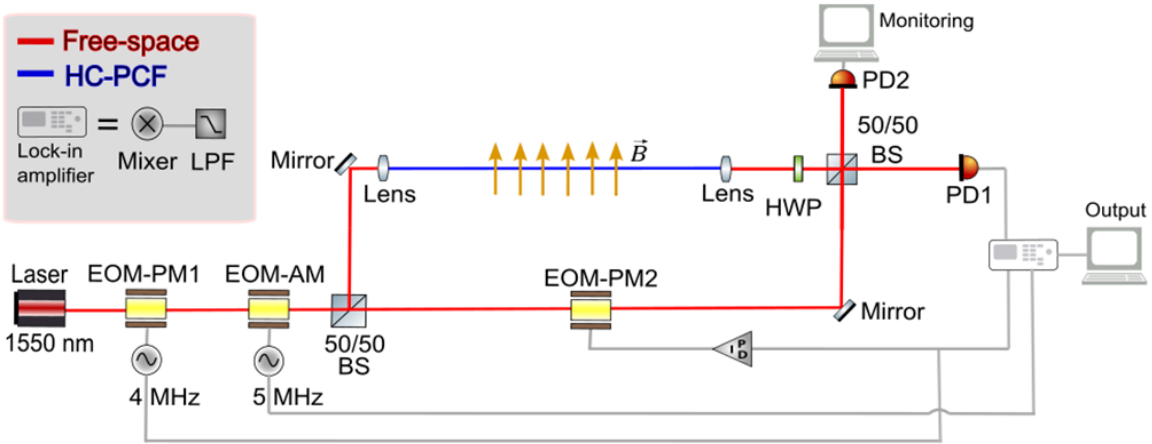

WISPFI Prototype – HC-PCF Integration

- R_c = 8.5 µm HC-PCF from MPI in Erlangen / Germany.
- Stable coupling to HC-PCF with ~80% efficiency.

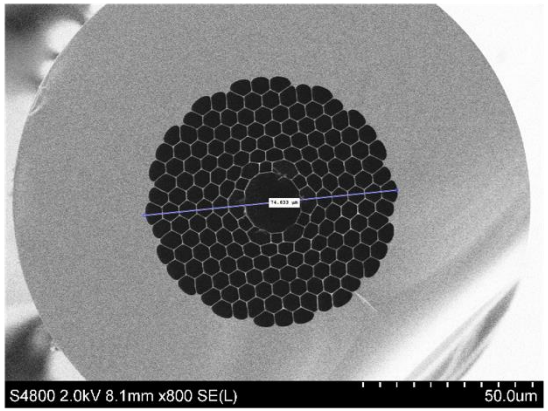

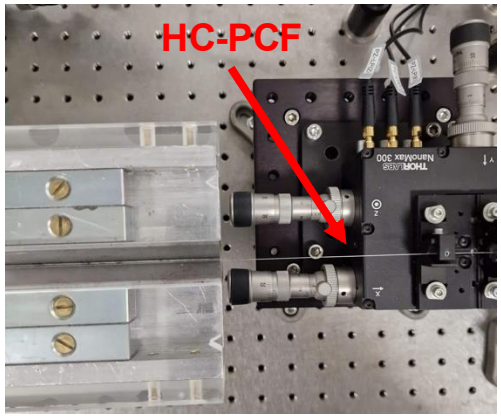

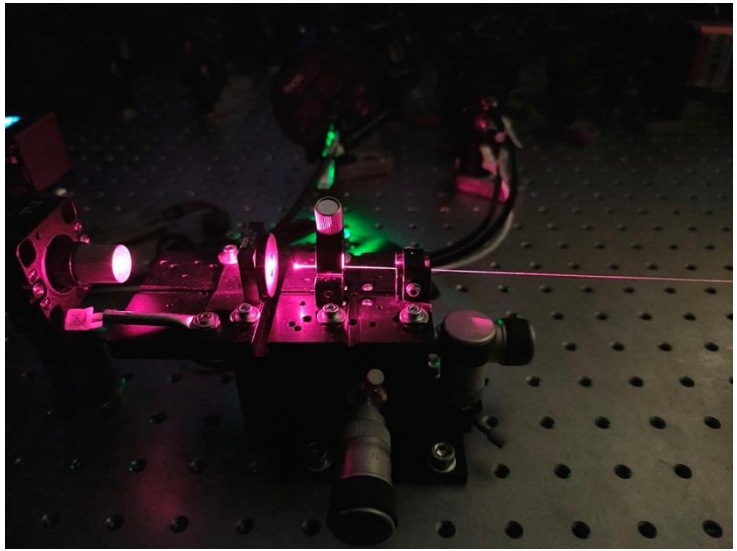

WISPFI Prototype – Magnet Panel

- Custom-made Alu panel consisting of 60 x Nd permanent magnets.
- 0.6 mm gap from Fe wedge to increase dipole field strength (2.4 T).
- Removable wedge to replace with Co-Fe alloy with even larger field line concentration (3.7 T).

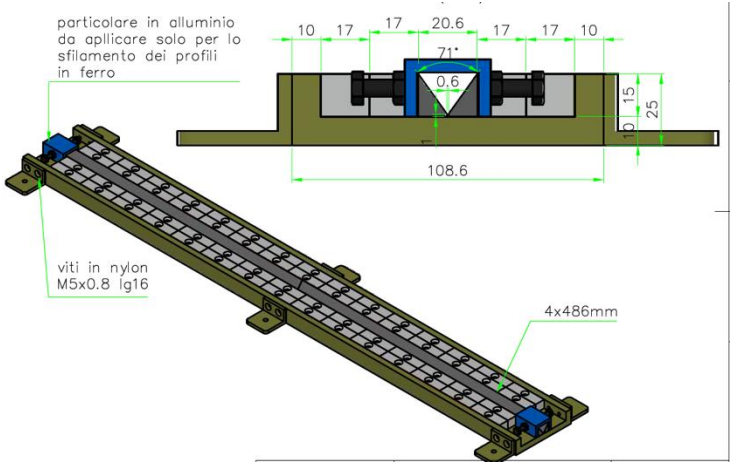

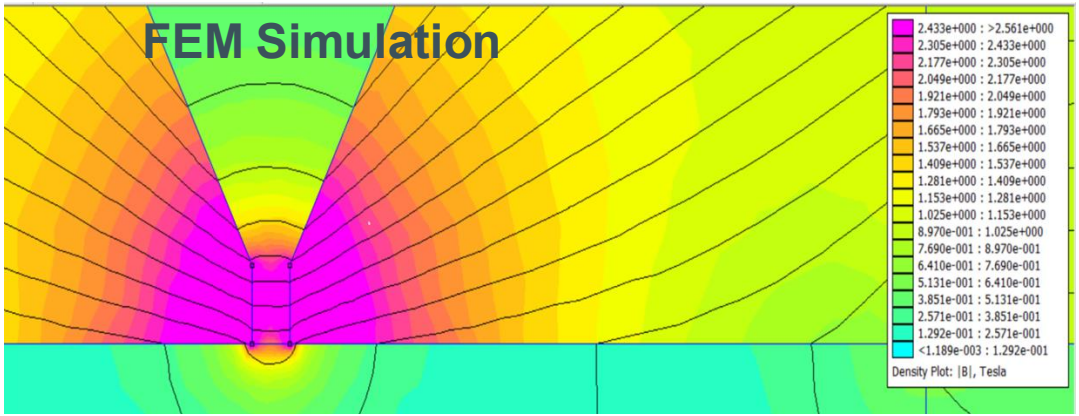

WISPFI Prototype – Magnet Panel

- Successful magnet integration including protection and custom-made mechanism for automatic B_ON and B_OFF measurements.

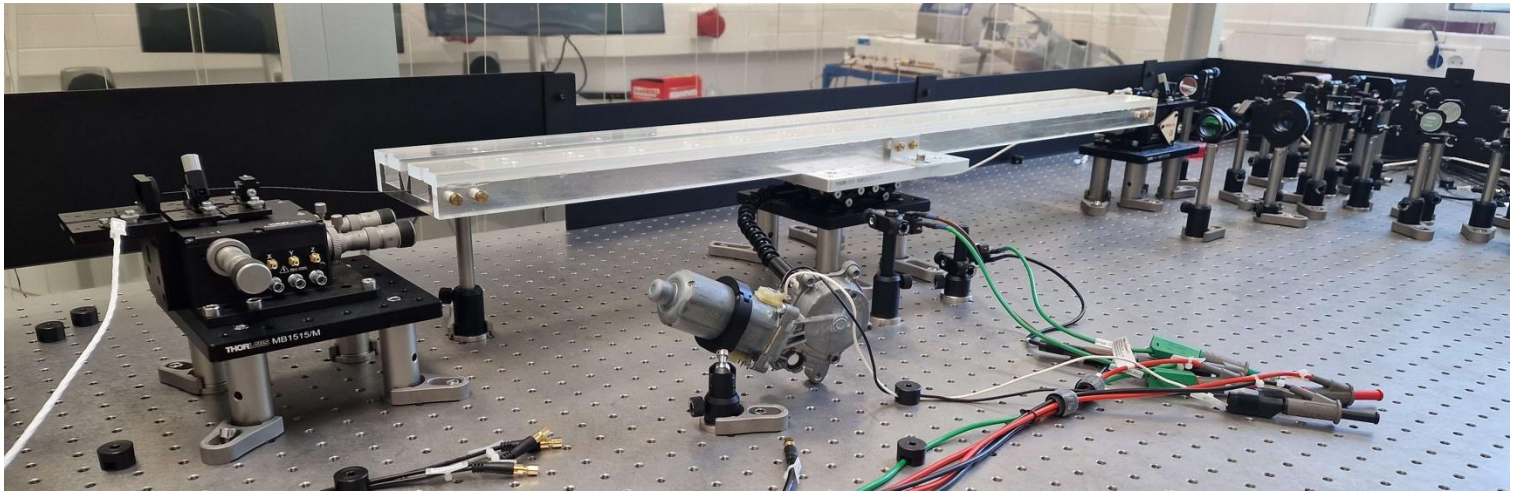

WISPFI Prototype – Magnet Panel

- Custom-made HC-PCF Alu holder design for secure straight mounting.
- Direct **B** measurement with transverse InAs Hall Sensor @ 1.6 T (reduced coverage).

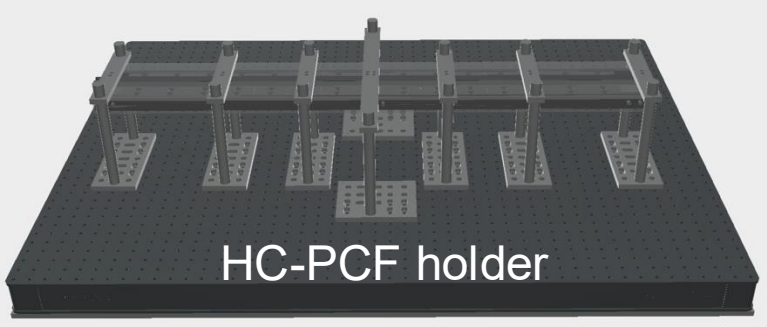

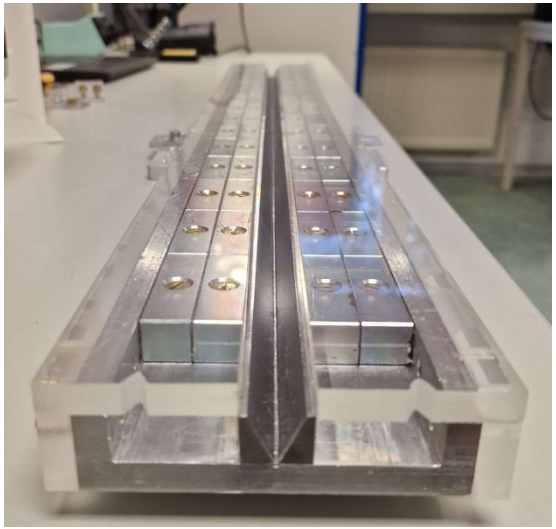

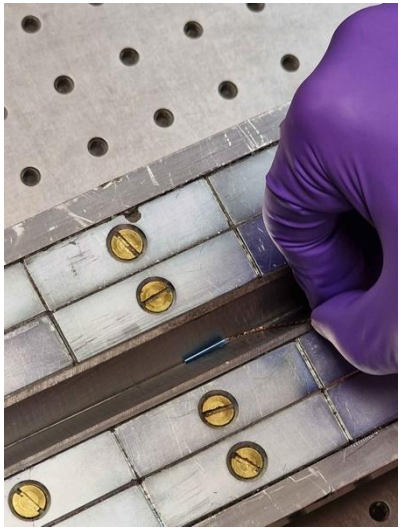

WISPFI Prototype – DAQ

- Fully automated DAQ system in python with multiple quality checks at various stages (polarization, beam profile, temperatures, etc).

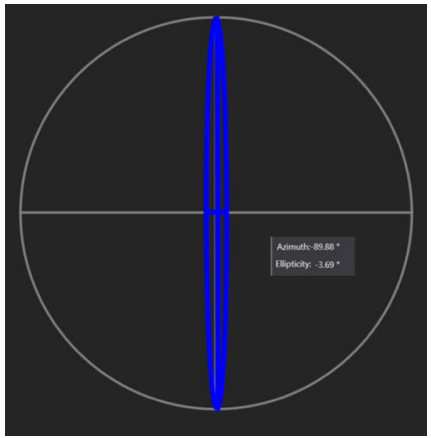

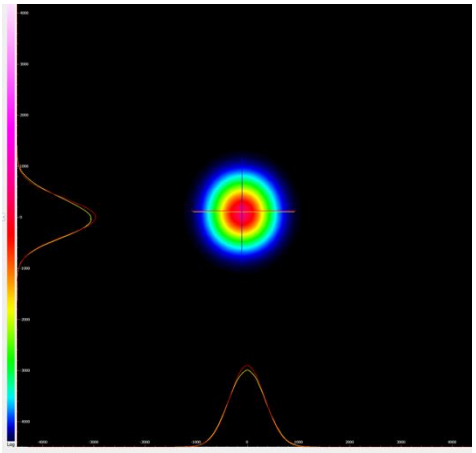

```
You are running DAQ_20240228.py

[INFO] [19:37:01] NKT 1550 nm laser is connected (25.2 °C).
[INFO] [19:37:02] NKT 1535 nm laser is connected (26.6 °C).
[INFO] [19:37:02] NKT 1570 nm laser is connected (26.2 °C).
[INFO] [19:37:03] Zurich Instruments Lock-in Amplifier is connected.
[INFO] [19:37:03] Rigol Signal Generator is connected.
[INFO] [19:37:03] Thorlabs Polarimeter PAX1000 is connected (35.1 °C).
[INFO] [19:37:03] Thorlabs Beam Profiler BP209 is connected.
[INFO] [19:37:06] Lakeshore Temperature Monitor 224 is connected.

Welcome to the Data Acquisition Shell of WISPFI! Type 'help' to see the available commands.
(daq) measure_beam_profile
[INFO] [19:37:10] Beam Profiler settings have been set.

Calculations Derived from Raw Data:
[INFO] [19:37:10] Peak position X: 282.67 µm.
[INFO] [19:37:10] Centroid position X: 273.43 µm.
[INFO] [19:37:10] Peak position in Y: -119.33 µm.
[INFO] [19:37:10] Centroid position Y: 5.58 µm.
[INFO] [19:37:10] Power is: 9.94 µW.

Profile Measurement:
[INFO] [19:37:10] Clip level is: 13.50% of peak.
[INFO] [19:37:10] Beam width X: 2671.97 µm.
[INFO] [19:37:10] Sigma width X: 744.28 µm.
[INFO] [19:37:10] Beam width Y: 3167.19 µm.
[INFO] [19:37:10] Sigma width Y: 815.99 µm.

Fit Measurement:
[INFO] [19:37:10] Gaussian amplitude X: 4607.01.
[INFO] [19:37:10] Gaussian diameter X: 2860.90 µm.
[INFO] [19:37:10] Gaussian fit percentage X: 94.74%.
[INFO] [19:37:10] Gaussian amplitude Y: 4002.56.
[INFO] [19:37:10] Gaussian diameter Y: 3134.82 µm.
[INFO] [19:37:10] Gaussian fit percentage Y: 97.08%.
```

WISPFI Prototype – Phase Locking

- Resonant EOM-PM for interferometer phase lock at ω_m = 4 MHz.
- Broadband EOM-PM adjusts the phase between the two arms and locks the interferometer in phase providing a stable working point for amplitude.
- Successful interferometer lock at 1% dark fringe for long period.

$$P_{out2}^{PM}(t) \approx 4E_0^2 J_1^2(\beta_m)\sin^2(\omega_m t - k_m L) - 2E_0^2 J_0(\beta_m) J_1(\beta_m) P_{\gamma\to a}\sin(\omega_m t - k_m L)$$

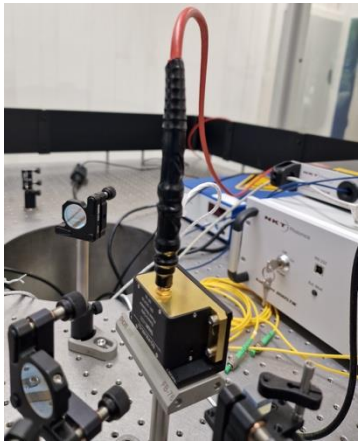

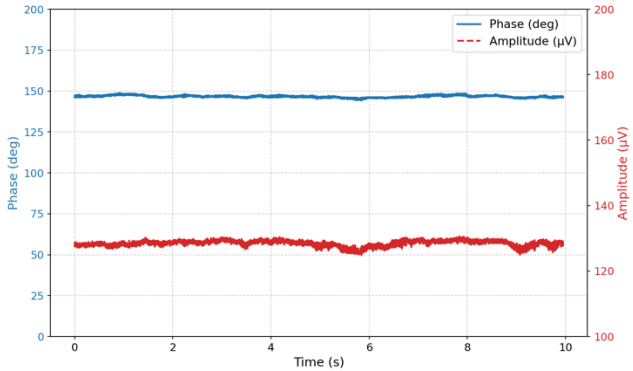

WISPFI Prototype – Latest Setup

- ✓ Successful transition to partial free space MZI (no step-index fiber).
- ✓ Efficient coupling to HC-PCF.
- ✓ Broadband EOM-PM for phase-locking (no fiber stretcher).
- ✓ Magnet integration and automatic B-ON/OFF measurements.
- ✓ Signal calibration via a dichroic mirror (amplitude reduction).
- ✓ Fully automatic DAQ system.

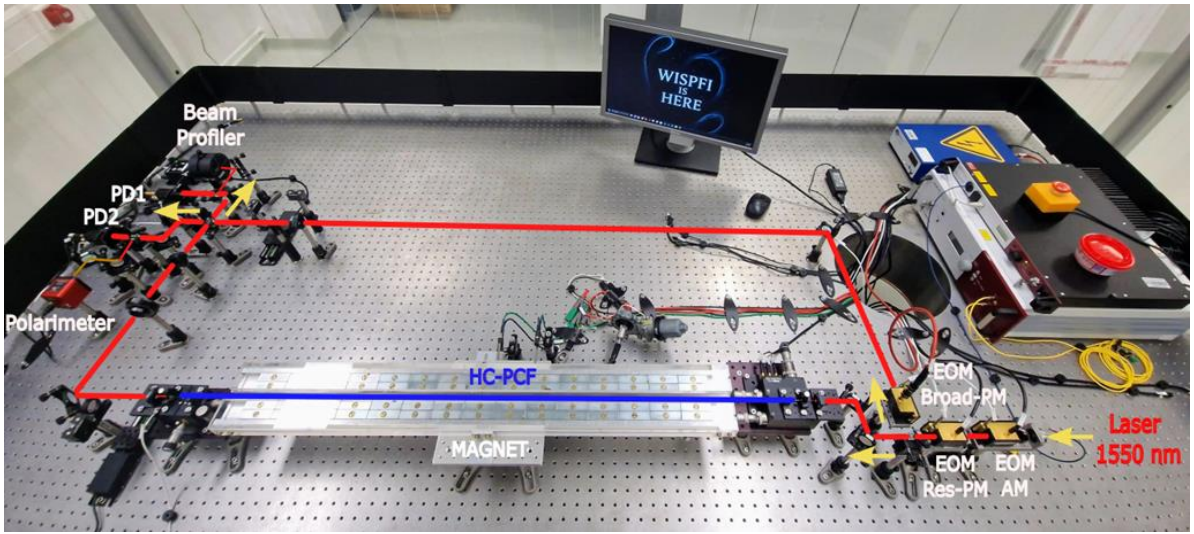

WISPFI Prototype – Projected Sensitivity

- WISPFI prototype sensitivity is projected to reach $g_{a\gamma\gamma} = 1.32 \times 10^{-9}$ GeV^{-1} at $m_a = 4.95 \times 10^{-2}$ μeV within 30 days.
- First model-independent table-top experiment exploring this frequency range.
- Test-bench for full WISPFI setup.

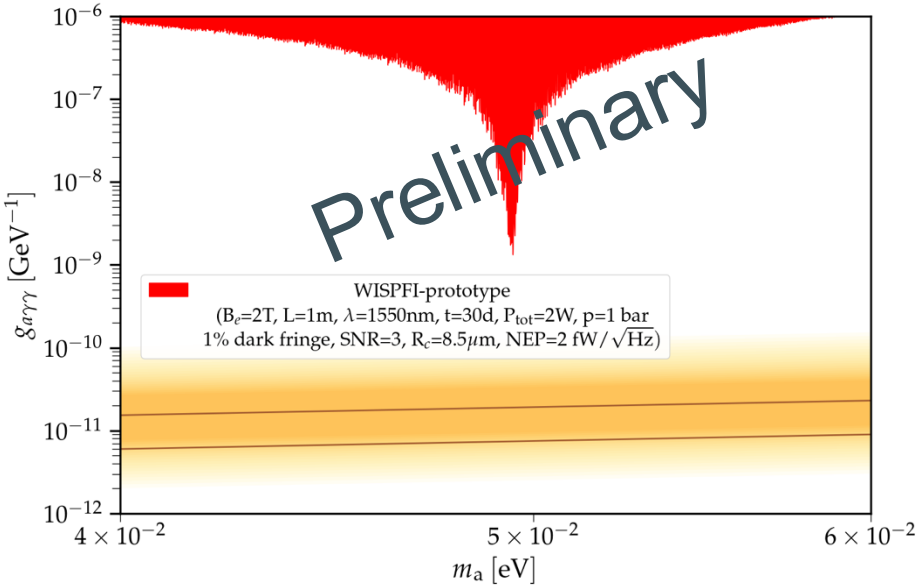

Future Steps

- Final commissioning and data acquisition for the WISPFI prototype setup.
- Data analysis and results setting a first $g_{a\gamma\gamma}$ limit in an unexplored region of the parameter space.
- Implementation of a pressure tuning procedure.
- Implementation of a FPC and final steps towards a full-scale WISPFI setup.

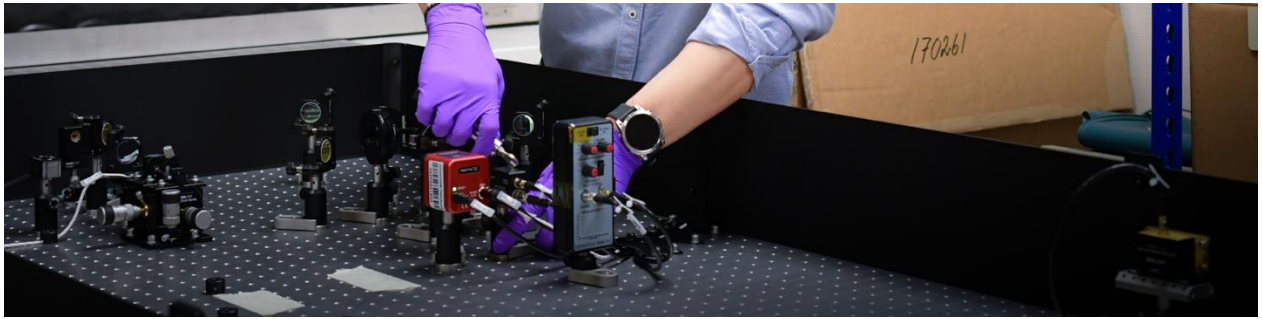

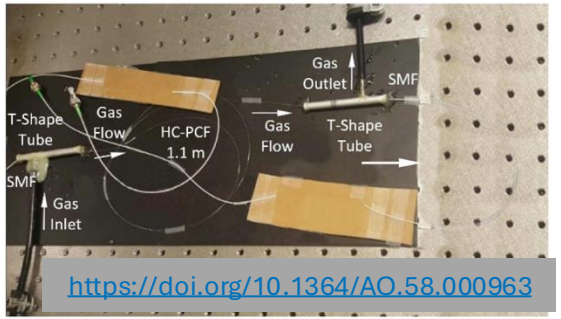

Fig. 5. Photo of HC-PCF connection to the gas flow.

Summary

- 1st **model-independent** experiment expected to reach the QCD axion at ~100meV.
- **Interferometric** technique with light propagation through **waveguide** in a strong magnetic field.
- Partial free-space, partial fiber **MZI**.
- **HC-PCF** meets the conditions for **resonant** mixing.
- **Amplitude reduction** in the presence of γ→a conversion.
- **Tuning** by regulating the **gas pressure** in the fiber.
- **Prototype** experiment **ready** to take data in UHH.

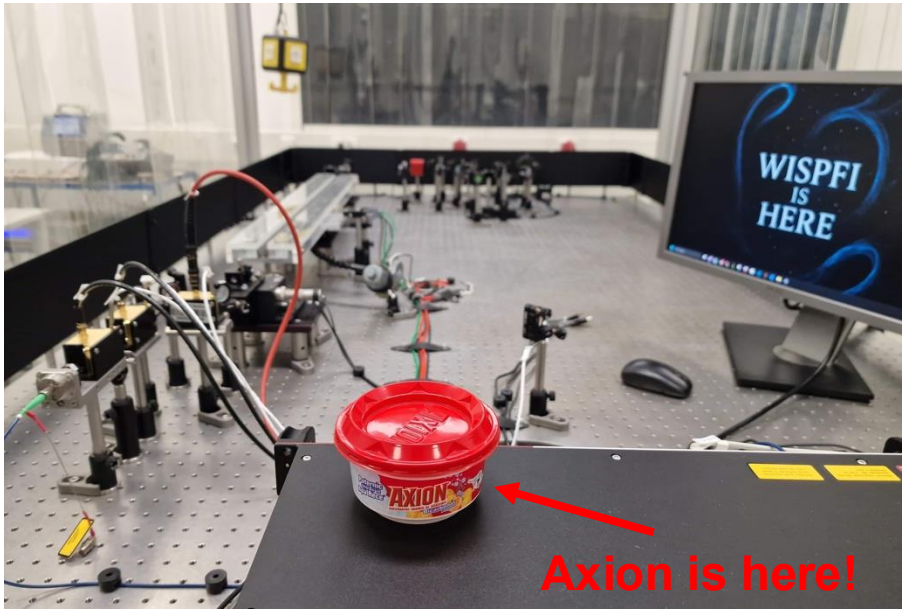

https://doi.org/10.1103/PhysRevD.109.123001

Universität Hamburg
DER FORSCHUNG | DER LEHRE | DER BILDUNG

CLUSTER OF EXCELLENCE
QUANTUM UNIVERSE

DESY.

Thanks for your attention!

Find out more about the cluster:
www.qu.uni-hamburg.de

References

1) R. D. Peccei, H. R. Quinn, CP Conservation in the Presence of Pseudoparticles, Phys. Rev. Lett. 38, 1440 (**1977**), https://doi.org/10.1103/PhysRevLett.38.1440
2) B. Eggemeier et al., Axion minivoids and implications for direct detection, Phys. Rev. D 107, 083510 (**2023**), https://doi.org/10.1103/PhysRevD.107.083510
3) V. Anastssopoulos et al., New CAST limit on the axion-photon interaction, Nature Phys.13, 584-590 (**2017**), https://doi.org/10.1038/nphys4109
4) J. M. Batllori, et al, WISP Searches on a Fiber Interferometer under a Strong Magnetic Field, arXiv (**2023**), https://doi.org/10.48550/arXiv.2305.12969
5) H. Tam, Q. Yang, Production and detection of axion-like particles by interferometry, Phys. Lett. B, 716, 435-440 (**2012**), https://doi.org/10.1016/j.physletb.2012.08.050
6) G. Raffelt, L. Stodolsky, Mixing of the photon with low-mass particles, Phys. Rev. D 37, 1237 (**1988**), https://doi.org/10.1103/PhysRevD.37.1237
7) P. Russell, Photonic Crystal Fibers, Science 299, 5605 (**2003**), https://doi.org/10.1126/science.1079280
8) E. A. J. Marcatili, R. A. Schmeltzer, Hollow Metallic and Dielectric Waveguides for Long Distance Optical Transmission and Lasers, Bell System Technical Journal 43, 4, (**1964**), https://doi.org/10.1002/j.1538-7305.1964.tb04108.x
9) L. Rosa et al., Analytical Formulas for Dispersion and Effective Area in Hollow-Core Tube Lattice Fibers, Fibers 9, 10, (**2021**), https://doi.org/10.3390/fib9100058
10) M. Ding et al., Hollow core fiber Fabry-Perot interferometers with finesse over 3000, Optica Publishing Group, (**2020**), https://doi.org/10.1364/CLEO_SI.2020.SF2P.2

Backup Slides

n_{eff} in HC-PCF (Confinement Losses)

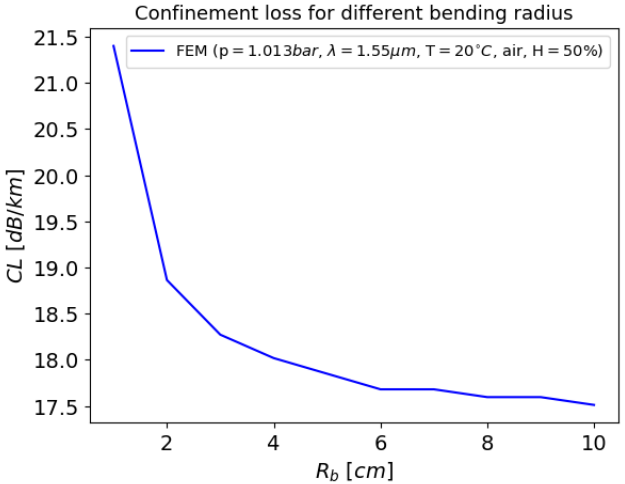

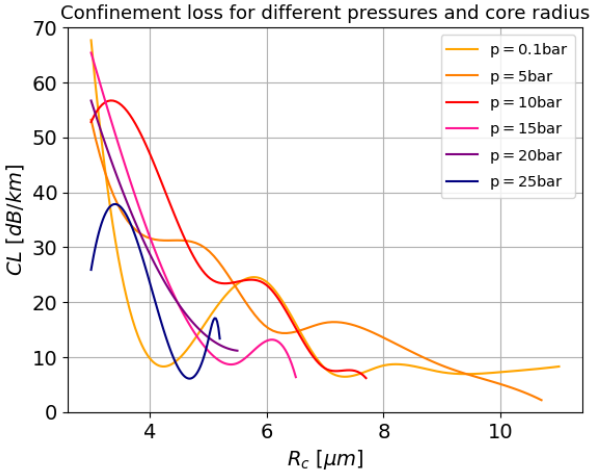

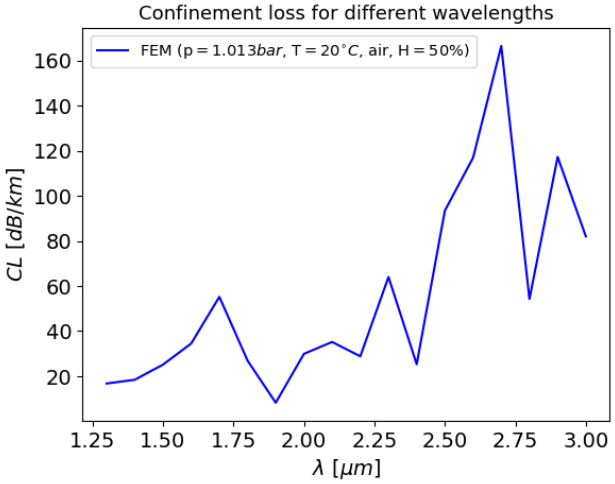

$$CL[dB/km] = -\frac{20}{\ln 10} \cdot \frac{2\pi}{\lambda} \cdot \mathrm{Im}(n_{eff})$$

Refractive index of air

- Refractive index of air as a function of pressure and temperature for T=20°C and P=1.013 bar accordingly.

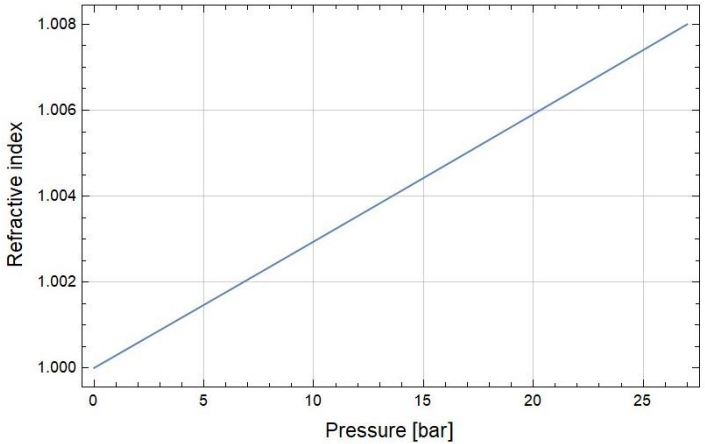

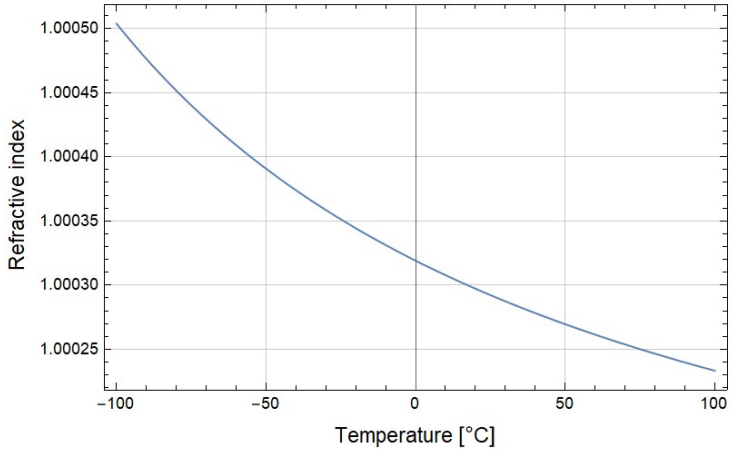

Photon-axion Conversion

- Original fields in terms of rotated fields:

$$\psi(z) = \begin{pmatrix} E(z) \\ a(z) \end{pmatrix} = U^{-1}(\theta)\,\tilde{\psi}(z), \quad \tilde{\psi}(z) = \begin{pmatrix} \tilde{E}(z) \\ \tilde{a}(z) \end{pmatrix}$$

- Conversion probability:

$$P_{\gamma\to a} = \frac{A_a^2}{I_T} = \cos^2\theta\,\sin^2\theta\left|e^{-i\tilde{k}_\gamma z} - e^{-i\tilde{k}_a z}\right|^2$$

- Simplified using oscillation wavenumber:

$$k_{\mathrm{osc}} = \tilde{k}_\gamma - \tilde{k}_a$$

$$\boxed{P_{\gamma\to a} = \sin^2(2\theta)\,\sin^2(k_{\mathrm{osc}} z)}$$